JOURNAL OF CATALYSIS 119, 467–482 (1989)

Isotopic Tracer and NMR Studies of Carbonaceous Species Present during CO Hydrogenation over Ru/TiO_2

G. H. YOKOMIZO AND A. T. BELL

Center for Advanced Materials, Lawrence Berkeley Laboratory, and Department of Chemical Engineering, University of California, Berkeley, California 94720

Received February 1, 1989; revised April 17, 1989

Isotopic tracer and NMR experiments have revealed the presence of carbidic carbon atoms and alkyl groups on a Ru/TiO_2 catalyst during CO hydrogenation. The carbidic carbon, which covers about 25% of the catalyst surface, is composed of two separate species, a methane precursor and a monomer building block for hydrocarbon chain growth. Modeling results indicate that both carbidic carbon species are formed directly from CO and that 80% of the carbidic carbon serves only as a monomer building block. The alkyl groups are divided into two separate species, C'_β and C''_β. The C'_β pool consists of the intermediates to C_{2+} hydrocarbon products, whereas the C''_β pool consists of longer alkyl chains which accumulate continuously during reaction and are believed to reside on the support.

INTRODUCTION

Isotopic tracer and NMR studies of CO hydrogenation over Ru/SiO_2 and Ru black conducted in this laboratory (*1–6*) have shown evidence for the presence of carbidic carbon and alkyl chains on the surface of Ru under reaction conditions. The surface concentration of carbidic carbon increases rapidly and comes to a steady-state level at the same time as the rate of product formation. Winslow and Bell (*2, 6*) have suggested that carbidic carbon is the primary precursor to the formation of methane and C_{2+} hydrocarbons. Based on isotopic tracer studies carried out with unsupported Co, Ni/SiO_2, and Ru/Al_2O_3, Biloen and coworkers (*7, 8*) concluded that only a small fraction of the total carbidic carbon may be active in the formation of methane. In subsequent work with unsupported Co and Ru/Al_2O_3, Zhang and Biloen (*9*) concluded that the carbidic carbon is divided into two pools, one containing the precursors to methane and the other, the monomeric building blocks required for hydrocarbon chain growth. From an analysis of isotopic tracer experiments with Co/SiO_2 and K-promoted Fe catalysts, Mims and McCandlish (*10, 11*) determined that the majority of the surface carbon is in the monomeric building block pool and that only a small fraction of the surface is occupied by growing hydrocarbon chains. More recently, Mims *et al.* (*12, 13*) have found evidence on Ru/Al_2O_3 for a long-lived C_2 species which behaves as a chain initiator. Stockwell *et al.* (*14*) have also reported recently that only a fraction of the active carbon present on the surface of an Fe/Al_2O_3 catalyst is involved in the formation of hydrocarbon products.

Alkyl chains have been observed on supported and unsupported Ru by both infrared and NMR spectroscopies (*4, 5, 15–22*) and have been found to accumulate during reaction to amounts exceeding the equivalent of a Ru monolayer (*17, 20, 22*). Since the alkyl species do not undergo H–D exchange under reaction conditions and are less reactive with hydrogen than carbidic carbon, several authors have proposed that the majority of the alkyl species are not involved in the mechanism of hydrocarbon synthesis (*15, 17, 18*). Other authors (*4, 16, 20*) on the other hand, have proposed that

0021-9517/89 $3.00

these species serve as reservoirs which resupply the catalyst surface with single carbon atoms.

The objective of this study was to characterize the dynamics of the deposition and reaction of carbonaceous species during CO hydrogenation over Ru/TiO_2. Titania was chosen as the support since Ru/TiO_2 has been found to be more active than Ru/SiO_2 or Ru/Al_2O_3 (*23*). One of the goals of this work was to compare the structure and reactivity of carbonaceous species deposited on Ru/TiO_2 with those of carbonaceous deposits formed on Ru/SiO_2 (*1, 2*). A second goal was to estimate what proportion of the alkyl chains observed under reaction conditions are active in the formation of C_{2+} hydrocarbons. The distribution of different carbonaceous species was investigated using isotopic tracer techniques in combination with temperature-programmed surface reaction (TPSR) spectroscopy and NMR spectroscopy.

EXPERIMENTAL

Three reactors were used in this study. Temperature-programmed surface reaction experiments were preformed in a low dead volume quartz tube. The reactor could be heated at a rate of 1 K/s. Infrared spectra of adsorbed CO were taken in a stainless-steel cell equipped with calcium fluoride windows (*24*). The preparation of samples for NMR spectroscopy was carried out in a 10-mm-o.d. pyrex tube with the ends fused to copper tubes. After sample preparation, the copper tubes were cold-welded and the reactor was placed inside the NMR spectrometer as explained in Ref. (*4*).

The experimental apparatus used has been described previously in Ref. (*2*). The flow system was designed to produce step function changes in isotopic composition of the gas mixture fed to one of the three reactors. Switching from isotopically labeled to unlabeled gas was accomplished using a computer-actuated, low dead volume, four-way valve. The time constant for the isotopic switch was less than 0.2 s. A portion of the product stream was sampled through a variable leak valve into a vacuum chamber containing a quadrupole mass spectrometer. The mass spectrometer was operated at an electron energy of 30 V to minimize the cracking of hydrocarbons. A microcomputer was used to schedule the gas delivery sequence, to select the mass spectrometer mass and gain settings, and to store the mass spectrometer signals as functions of time.

The ^{13}C NMR experiments were performed on a Bruker CXP-200 spectrometer, operating at 50.34 MHz. The magic angle spinning ^{13}C NMR was preformed in a 180 MHz homebuilt spectrometer. The sample was transferred from the reactor into a Macor rotor in a dry box under argon atmosphere. A Doty Scientific magic angle spinning NMR probe was used.

H_2, CO, and He were supplied to the reactor from a gas manifold. UHP hydrogen from Matheson was purified by passage through a Deoxo purifier (Engelhard) and molecular sieves (Linde 13×) cooled in dry ice. Helium obtained from the Lawrence Berkeley Laboratory was purified by passage through Oxy-Absorbent (Alltech Associates) and molecular sieves cooled in dry ice. UHP carbon monoxide from Matheson was purified of iron carbonyls by passage through a copper tube packed with glass beads and heated to 473 K. Further purification was accomplished by passage through Ascarite and molecular-sieve-cooled in dry ice. Isotopically labeled 99% ^{13}CO was obtained from Isotec and used without further purification.

A 4.3% Ru/TiO_2 catalyst was prepared by incipient wetness impregnation of Titania P-25 (Degussa) with an aqueous solution of $RuCl_3 \cdot 3H_2O$ (Strem). The impregnated support was dried in air at 373 K overnight. The catalyst was sieved to −30, +60 mesh particles. Reduction of the catalyst was carried out in the quartz reactor. The reactor was loaded with 50 mg of catalyst and the temperature was ramped at 0.2 K/s to 573 K under flowing hydrogen. The temperature

was then maintained at 573 K for 2 h, after which the sample was flushed for 30 min at 573 K in flowing He to remove chemisorbed hydrogen. The dispersion of Ru was determined by hydrogen chemisorption at 373 K following reduction at 473 K and was found to be 12%.

A standard experimental procedure was used for this study. The catalyst was first reduced in flowing H_2 and then exposed to the desired reaction gas to label isotopically the carbon species of interest. All experiments were carried out using a CO partial pressure of 50 Torr and a D_2 partial pressure of 150 Torr, at a total pressure of 760 Torr. Following a reaction sequence, the reactor was flushed with helium to remove gas-phase reactants. The catalyst was then quenched to room temperature in approximately 20 s by blowing N_2, gas-cooled in liquid N_2, over the outside of the reactor. To characterize the carbonaceous species remaining on the catalyst, the catalyst was then heated at 1 K/s in flowing deuterium and the production of ^{13}C-labeled products was monitored.

The steady-state product distribution was measured by gas chromatography using a Varian Model 3700 GC equipped with a FID. C_1–C_7 hydrocarbons were resolved on a 2-m-long, teflon-coated $\frac{1}{8}$-in. stainless-steel tube packed with Porapak PS (*25*). The product distribution was measured after 5 min of reaction. The products followed a Shulz–Flory–Anderson (SFA) distribution characterized by $\alpha = 0.69$.

RESULTS

The following procedure was used to determine the reactivity of chemisorbed CO. The reduced catalyst was flushed with helium for 30 min at 573 K to removed absorbed hydrogen and then exposed to ^{13}CO for 30 s at 50 Torr at room temperature. The sample was flushed with helium for 10 min and then the temperature was ramped at 1 K/s in 150 Torr of deuterium. The total flow rate of gas was 152 cm^3/min. The major product observed was methane. The rate of methane formation passed through a maximum at 419 K as shown by spectrum (a) in Fig. 1. The CO coverage calculated by integrating the methane peak was 1.05 of a Ru monolayer. Trace amounts of ethane were also observed, but no carbon monoxide was detected.

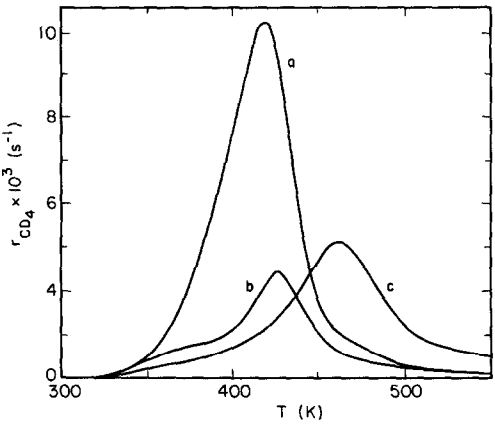

FIG. 1. Comparison of ^{13}C TPSR spectra for (a) adsorbed CO, (b) Boudouard carbon, (c) ^{13}C-labeled Boudouard carbon exposed to ^{12}CO and D_2 for 25 s.

Labeled ^{13}C was deposited on the surface by flowing 50 Torr of ^{13}CO for 300 s at 463 K over a sample previously flushed in He at 673 K. Production of CO_2 was observed indicating carbon deposition by the Boudouard reaction. ^{12}CO was then flowed over the catalyst for 25 s to exchange with the chemisorbed ^{13}CO. *In situ* infrared spectra showed that the CO isotopic exchange occurred in less than 2 s. Upon heating the catalyst in deuterium, the major labeled product observed was methane. Spectrum (b) in Fig. 1 shows the rate of methane formation as a function of temperature. The maximum rate occurs at 427 K and a shoulder can be seen at 378 K. The total amount of ^{13}C-labeled carbon removed from the surface is 0.33 ML (monolayers). In a separate experiment, the catalyst was again exposed to ^{13}CO for 300 s at 463 K, but then treated with a 3 : 1 mixture of D_2 and ^{12}CO for 25 s. The subsequent temperature-programmed reaction spectrum showed the major labeled peak to be meth-

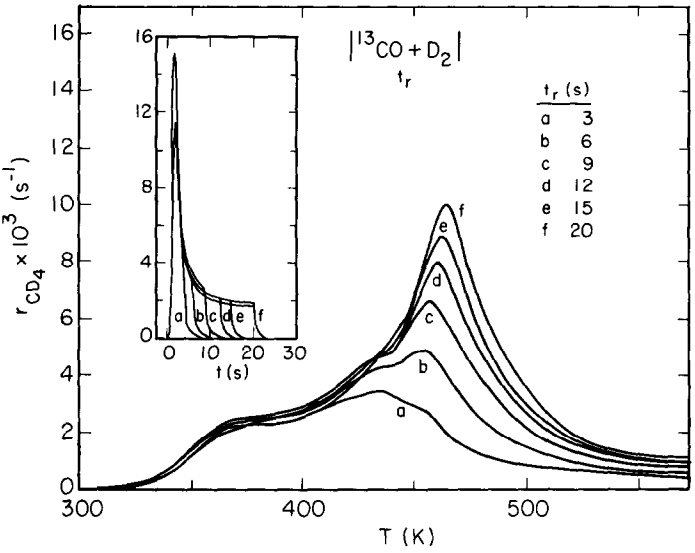

FIG. 2. Effect of reaction time on ^{13}C TPSR spectra of C_α and C_β. Inset: The rate of $^{13}CD_4$ formation observed during initial exposure to ^{13}CO and D_2. Reaction conditions: P_{D_2} = 150 Torr, P_{CO} = 50 Torr, T = 463 K. Gas introduction sequence: $^{13}CO + D_2$ (t_r) → ^{12}CO + He (25 s) → He (cool) → D_2 (TPR).

ane with a peak maximum at 463 K (see Fig. 1). The total amount of ^{13}C-labeled carbon removed in this instance was 0.5 ML.

The buildup of surface carbon under reaction conditions was studied for an initially reduced catalyst and for a catalyst operating under steady-state conditions. In the first case, a 3 : 1 mixture of D_2 and ^{13}CO (150 Torr D_2 and 50 Torr CO) was passed over the freshly reduced catalyst for 3 to 20 s. The reaction temperature for these experiments was 463 K. The rate of methanation as a function of reaction time is shown in the inset in Fig. 2. After a fixed reaction time, the chemisorbed ^{13}CO was replaced with ^{12}CO by exposing the catalyst to a flow of ^{12}CO for 25 s. The reactor was then flushed with He and the TPSR spectrum recorded in the presence of flowing D_2. The principal product observed was CD_4 and only small amounts of higher hydrocarbons were detected. Figure 2 shows a series of TPSR spectra recorded following progressively longer exposure of the catalyst to the reaction mixture. These spectra consist of two overlapping peaks. The peak at 400 K reaches a maximum intensity almost instantaneously. The second peak evolves more slowly and continues to grow even after 30 s of exposure of the catalyst to the reaction mixture. The temperature for the maximum of this peak appears to shift from 453 to 463 K with increasing duration under reaction conditions.

The amount of surface carbon accumulated after 3 s of reaction is approximately 0.25 ML, as determined by integration of the corresponding TPSR spectrum shown in Fig. 2. The shape of this spectrum and the location of the maxima are very similar to those for the spectrum of Boudouard carbon, shown in Fig. 1. Since Boudouard carbon is devoid of any hydrogen, the majority of the carbon deposited after 3 s of reaction is designated as C_α, using the nomenclature of Winslow and Bell (*2*). As will be demonstrated below, this assignment is supported by NMR spectra of the deposited carbon.

The methane peak which appears between 463 and 473 K with increasing reaction time (see Fig. 2) occurs in the same temperature range as the TPSR peak observed in Fig. 1 obtained following exposure of Boudouard carbon to a mixture of

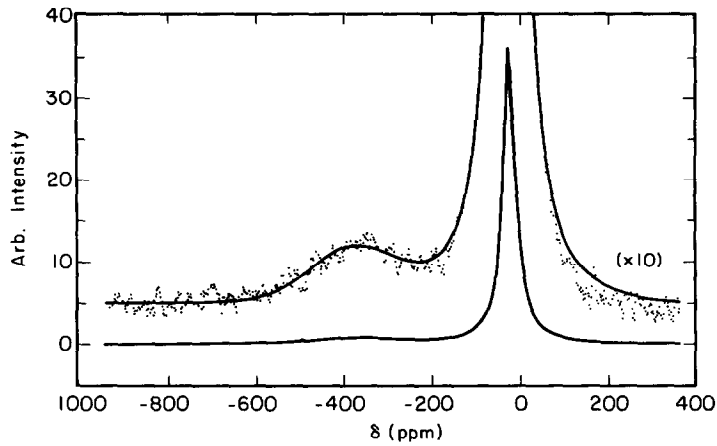

FIG. 3. ^{13}C NMR spectrum of carbonaceous species deposited on after 120 s of steady-state reaction in $^{13}CO/D_2$.

CO and D_2. As discussed below, this peak can be attributed to the presence of alkyl groups on the catalyst surface, and hence is ascribed to C_β, using the notation of Winslow and Bell (*2*). The amount of C_β accumulated after 30 s is 1.7 ML, and this amount grows to greater than 3 ML if the reaction is allowed to continue for 120 s.

^{13}C NMR spectra of the carbonaceous deposits were recorded to confirm the presence of C_α and C_β on the catalyst surface. Figure 3 illustrates the spectrum obtained after exposure of the catalyst to reaction conditions for 120 s. The appearance of this spectrum is very similar to those reported by Duncan *et al.* (*4*) for CO hydrogenation over Ru/SiO_2. By analogy with the work of these authors, the broad peak at 346 ppm can be assigned to C_α and the narrow peak at 9.5 ppm, to C_β. Magic angle spinning NMR spectroscopy showed that the narrow peak could be decomposed into five components, revealing the presence of $-CH_2-$ and $-CH_3$ groups in different environments. As noted in Table 1, the position of the MAS–NMR peaks are consistent with the results reported by Duncan *et al.* (*5*) for Ru/SiO_2.

The dynamics of carbon accumulation under steady-state conditions were investigated in the following manner. Steady-state methanation was established by flowing ^{12}CO and D_2 for 30 s. The reactant mixture was then switched to one containing ^{13}CO and D_2 for 2 to 30 s. Adsorbed ^{13}CO was displaced from the catalyst surface by passing ^{12}CO through the reactor for 25 s. Following a short flush of the reactor with He, the ^{13}C-labeled carbon was reacted in flowing D_2.

Figure 4 shows the rate of $^{13}CD_4$ formation during the period following the switch in feed composition from $^{12}CO/D_2$ to $^{13}CO/D_2$ and the corresponding TPSR spectra of the surface carbon. The rate of replacement of the $^{12}CD_4$ with $^{13}CD_4$ is characterized by a half-life ($t_{1/2}$) of 4.9 s. While the appearance of the TPSR spectra in Fig. 4 is similar to those shown in Fig. 2, the change in relative peak intensities with time under reaction conditions is different. The principal

TABLE 1

^{13}C NMR Spectra Assignments[a]

Center of mass (this study)	Center of mass (Duncan *et al.* (*5*))	Assignment
—	35.1	$Ru-C^*H_2-CH_2-$
28.7	28.3	$Ru-CH_2-(C^*H_2)_n-CH_2-CH_3$
20.1	21.1	$Ru-CH_2-(CH_2)_n-C^*H_2-CH_3$
—	18.4	$Ru-CH_2-C^*H_2-CH_3$(?)
11.0	11.7	$-CH_2-C^*H_3$

[a] In ppm.

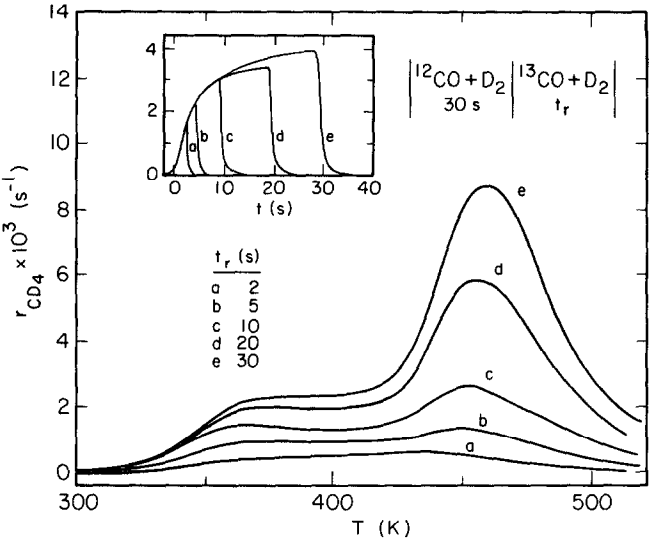

FIG. 4. Effect on ^{13}C TPSR spectra of the duration of exposure to $^{13}CO/D_2$ after exposure to $^{12}CO/D_2$ for 30 s. Reaction conditions: P_{D_2} = 150 Torr, P_{CO} = 50 Torr, T = 463 K. Gas introduction sequence: $^{12}CO + D_2$ (30 s) → $^{13}CO + D_2$ (t_r) → ^{13}CO (25 s) → He (cool) → D_2 (TPR).

distinction is that the accumulation of C_α (i.e., carbon reacting between 323 and 423 K) occurs more slowly under steady-state conditions than over a freshly reduced catalyst. In fact, the spectra shown in Fig. 4 demonstrate that 20 to 30 s are required for the steady-state inventory of C_α to be established, whereas only 3 s are required during startup of the reaction over a freshly reduced catalyst. However, as in Fig. 2, the build up of C_β increases monotonically. A further point of note is that the accumulation of C_α reaches a plateau at about the same time that the rate of CD_4 formation reaches steady state.

The path of labeled carbon during steady-state reaction was investigated by exposing the catalyst to a $^{13}CO/D_2$ mixture for 30 s and then switching over to a mixture of $^{12}CO/D_2$. The subsequent TPSR spectra are shown in Fig. 5. It is apparent that $^{13}C_\alpha$ reacts rapidly and is almost totally removed after 50 s under $^{12}CO/D_2$. Concurrently, there is a slight increase in the intensity of the C_β peak. This is then followed by a decrease in the C_β peak intensity and a shift of the peak maximum to higher temperatures. Quite surprisingly, though, after 200 s of reaction in ^{12}CO and D_2, the intensity of the C_β peak remains constant, while the position of this peak continues to shift upscale. Figure 6 illustrates ^{13}C NMR spectra taken immediately after preparation (spectrum (a)), and after exposure of the catalyst to a ^{12}CO and D_2 mixture for 90 s (spectrum (b)). It is evident that in the latter case the C_α peak is totally absent, whereas the C_β peak has virtually the same intensity in both cases. These experiments lend further confirmation to the assignment of the low-temperature portion of the TPSR spectra to C_α shown in Figs. 2 and 4.

The effects of thermal aging on the reactivity of C_α and C_β were investigated by allowing the freshly formed surface carbon to stand in He at reaction temperature for 0 to 800 s before obtaining a TPSR spectrum. The results of these experiments are shown in Fig. 7. With increasing aging at 463 K, the C_β peak centered at 463 K decreases in intensity, but the total amount of reactive carbon remains constant. These results suggest that with aging, C_β forms a more refractory type of carbon.

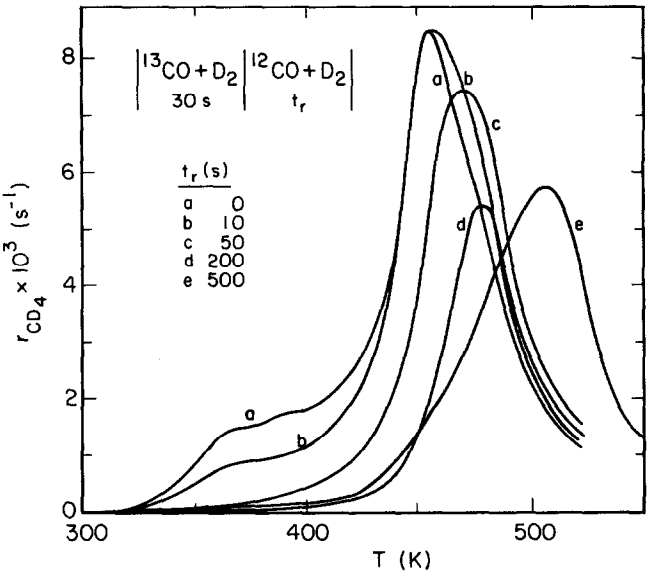

FIG. 5. Effect on ^{13}C TPSR spectra of the duration of exposure to $^{12}CO/D_2$ after initial exposure to $^{13}CO/D_2$ for 30 s. Reaction conditions: P_{D_2} = 150 Torr, P_{CO} = 50 Torr, T = 463 K. Gas introduction sequence: $^{13}CO + D_2$ (30 s) → $^{12}CO + D_2$ (t_r) → ^{13}CO (25 s) → He (cool) → D_2 (TPR).

Experiments were also carried out to determine the effects of aging on the components of C_β remaining on the catalyst surface after extensive reaction of the ^{13}C-labeled carbon deposit in a $^{12}CO/D_2$ mixture. Figure 8 shows that this form of carbon is essentially unaffected by aging in He and will be referred to as C''_β. The alkyl chains which are removed from the catalyst surface during steady-state reaction will be referred to as C'_β.

NMR spectroscopy was used in an effort to differentiate between C'_β and C''_β. Spectra of catalysts samples with C'_β and C''_β are shown in Fig. 9. Also shown is a difference spectrum obtained after normalization of

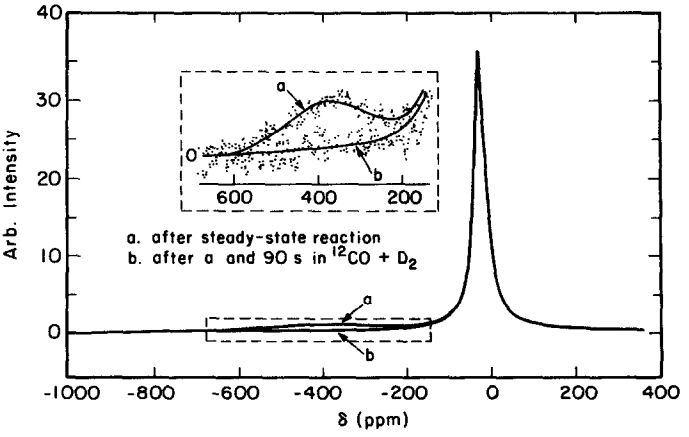

FIG. 6. ^{13}C NMR spectrum of carbonaceous species: (a) after 120 s of steady-state reaction in $^{13}CO/D_2$; (b) following (a) after 90 s of exposure to $^{12}CO/D_2$.

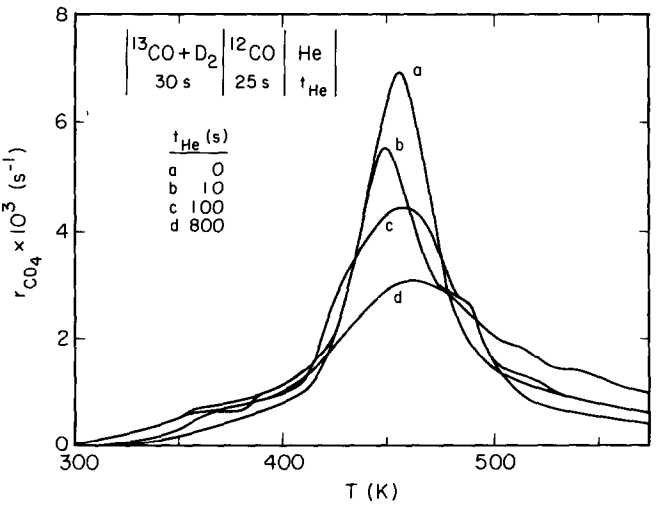

FIG. 7. Effect on ^{13}C TPSR spectra of the duration of He flushing. Reaction conditions: P_{D_2} = 150 Torr, P_{CO} = 50 Torr, T = 463 K. Gas introduction sequence: $^{13}CO + D_2$ (30 s) → ^{12}CO + He (25 s) → He (t_{He}) → D_2 (TPR).

the peak areas. The difference spectrum indicates that C''_β has a larger amount of carbon at 28 ppm. Carbon exhibiting a peak at 28 ppm has previously been assigned to CH_2 groups in linear alkyl chains (*5*). This suggests that the length of alkyl chains comprising C''_β is longer than that of the chains comprising C'_β. MAS–NMR spectra show that the ratio of CH_3/CH_2 groups is smaller for C''_β than C'_β, also indicating that C''_β consists of longer carbon chains.

DISCUSSION

Winslow and Bell (*2, 6*) have concluded that on Ru/SiO_2, C_α is the precursor to methane. The results of this study indicate

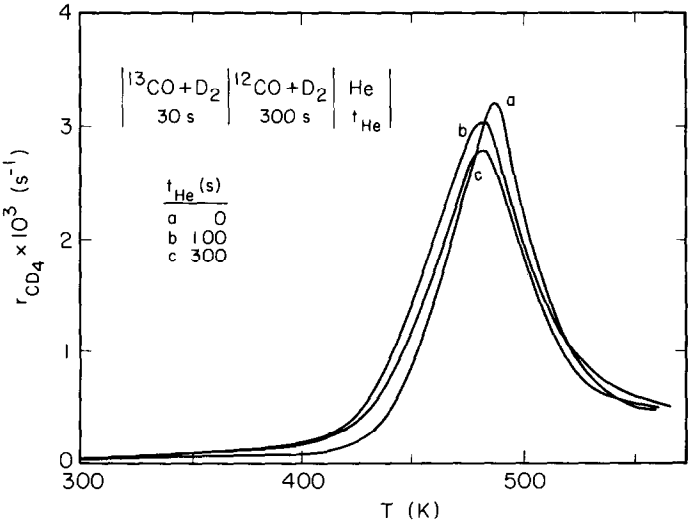

FIG. 8. Effect on ^{13}C TPSR spectra of the duration of He flushing. Reaction conditions: P_{D_2} = 150 Torr, P_{CO} = 50 Torr, T = 463 K. Gas introduction sequence: $^{13}CO + D_2$ (30 s) → $^{12}CO + D_2$ (300 s) → He (t_{He}) → D_2 (TPR).

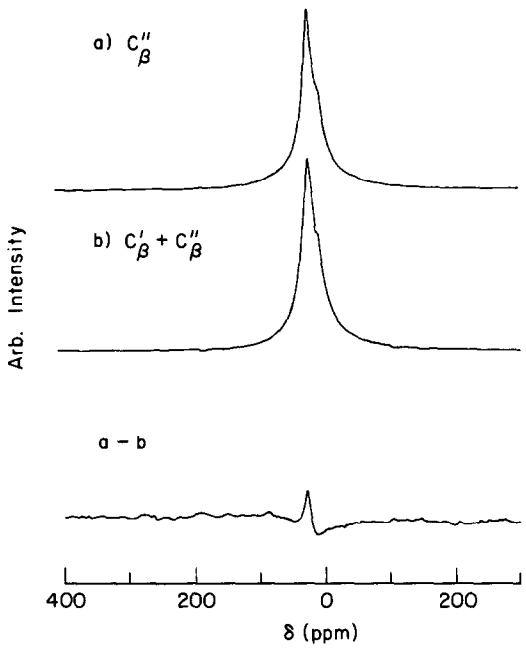

FIG. 9. ^{13}C NMR spectrum of carbonaceous species (a) after 120 s of steady-state reaction in $^{13}CO/D_2$ followed by 90 s of exposure to $^{12}CO/D_2$; (b) after 120 s of steady-state reaction in $^{13}CO/D_2$ followed by 500 s of exposure to $^{12}CO/D_2$.

that an identical conclusion can be drawn for methane formation over Ru/TiO_2. As seen in Fig. 2, the rate of methane formation reaches a steady-state level at the same time as the surface coverage by C_α. Similarly, Fig. 4 shows that the surface coverage of $^{13}C_\alpha$ and the rate of formation of ^{13}C-labeled methane reach a steady state at the same time.

The C'_β pool is believed to consist of the precursors to paraffins and olefins. The rate of removal of the C'_β from the surface during steady-state reaction is estimated from the data presented in Fig. 5. After a known amount of $^{13}C_\beta$ is deposited on the catalyst surface, the amount of $^{13}C_\beta$ remaining as a function of reaction time in ^{12}CO and D_2 is measured. Since the rate of $^{13}C'_\beta$ removal is seven times faster than the rate of labeled methane formation, one may conclude that C'_β leaves the surface as C_{2+} products, and hence, that C'_β consists of the precursors to C_{2+} products.

The C''_β pool of carbon probably contains longer hydrocarbon chains which may be present on either the metal or the catalyst support. NMR spectra (see Fig. 9) have shown that the C''_β chains are longer than the C'_β chains. The amount of C''_β increases with reaction time without significantly decreasing the reaction rate suggesting that the chains do not block a significant portion of the Ru surface. Further evidence for the contention that C''_β resides primarily on the support is provided by the data presented in Figs. 7 and 8, which show that the C''_β is stable during He aging whereas the C'_β becomes more refractory with aging at 463 K. Previous studies using *in situ* infrared spectroscopy have shown that hydrocarbon chains accumulate on supported Ru catalysts during CO hydrogenation (*15–22*) and that these chains are not affected by purging in He (*17, 18*). In addition, the wax buildup on Ru/Al_2O_3 has been shown to consist of C_{30+} hydrocarbon chains which have the same carbon number distribution as the reaction products, suggesting that the very long hydrocarbon chains produced are trapped on the catalyst surface (*26*). Fukushima *et al.* (*21*) have shown with infrared spectroscopy that chains accumulating on the catalyst surface have a greater proportion of $-CH_2-$ groups than the reaction products, in agreement with the results of NMR spectroscopy presented here. The retention of hydrocarbon chains longer than C_9 during CO hydrogenation over Ru supported on microporous silica has also been observed by Wakui and Handa (*27*).

The methane peak observed during the TPSR of C_β can be ascribed to the hydrogenolysis of alkyl chains. This interpretation is suggested by the infrared observations of Tamaru and co-workers (*20*) who found a decrease in alkyl chain length during the isothermal reduction of alkyl groups formed on a Ru/SiO_2 catalyst by CO hydrogenation. More recently, Zhou and Gulari (*28*) have shown that H_2 reduction of C_β

results in a spectrum of hydrocarbon products, but that this spectrum does not follow an SFA distribution. It was concluded, therefore, that the reduction of C_β proceeds by hydrogenolysis of alkyl chains.

Since the hydrogenolysis of alkyl chains requires Ru sites but the majority of the C_β inventory is stored on the support, the consumption of C_β during TPSR must occur as a consequence of surface diffusion of the species composing C_β from the support to the dispersed Ru particles. It is also noted that the temperature at which C_β reacts is higher than that at which adsorbed CO undergoes hydrogenation. This is believed to be due to the stabilization of the alkyl chains composing C_β by adsorbed CO. Consistent with this, Akhter and White (*29*) have shown that C_2D_x fragments are stabilized by adsorbed CO on Ni(100).

The conversion of C_α to C_β during reaction is shown clearly in Fig. 1 and has been previously reported by Winslow and Bell (*2*). The addition of hydrogen to the Boudouard carbon changes the TPSR peak position from that for C_α to that for C_β. Examination of Fig. 5 also shows that after the isotopic switch to ^{12}CO and D_2, the amount of $^{13}C_\alpha$ decreases and the amount of $^{13}C_\beta$ increases during the first 10 s of reaction in the $^{12}CO/D_2$ mixture. Since the $^{13}C_\alpha$ is the only source of labeled carbon on the catalyst surface, the increase in the amount of $^{13}C_\beta$ must be from the conversion of $^{13}C_\alpha$ to $^{13}C_\beta$. In addition, during the start-up of reaction, C_β formation does not occur until after C_α is formed (see Fig. 2). The addition of hydrogen to the Boudouard carbon changes the TPSR peak position from that for C_α to that for C_β.

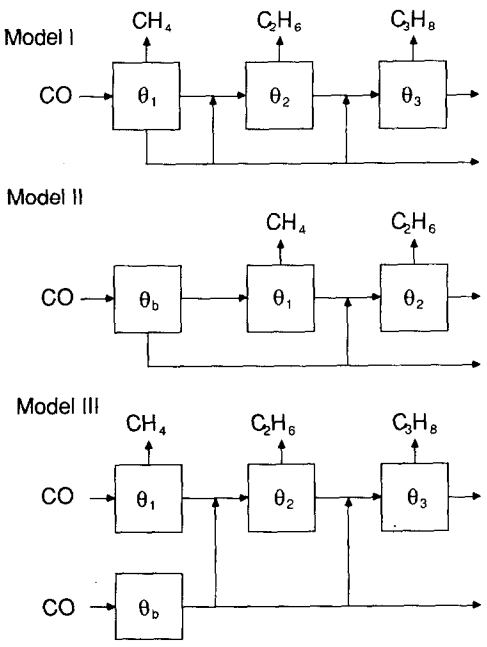

FIG. 10. Proposed models for the relationship between the methane precursor and the monomer building block in the mechanism of CO hydrogenation.

To obtain additional insights into the reaction mechanism, the experimental results were compared with three different models. Each of these models is presented schematically in Fig. 10. Model I has one pool of monomer carbon, θ_1, which contains the precursor to methane and the building blocks to form hydrocarbon chains. This model is suggested by the observation of only one type of carbidic carbon (C_α) by TPSR and NMR spectroscopy. Model II is that proposed by Zhang and Biloen (*9*) to account for the product distribution observed during transient isotopic tracer experiments. The C_α is divided into two separate pools, the methane precursor (θ_1) and the monomer building block (θ_b). The methane precursor is formed from the monomer building block. Model III also separates the C_α into methane precursor and building-block pools, but in contrast to Model II, the methane precursor is formed directly from CO.

As discussed in the Appendix, each of the models involves four parameters: α, $t_{1/2}$, k_t, and θ_b/θ_1. The parameters α and $t_{1/2}$ can be measured directly from experimental data and are reported in Table 2. The confidence limits on these measurements are 95%. The remaining two parameters are the rate coefficient for termination, k_t, and the ratio of the surface coverage of monomer building block to that of the methane

TABLE 2

Modeling Parameters

$\alpha = 0.69 \pm 0.04$
$t_{1/2} = 4.9 \pm 0.5$ s
$r_1/\theta_\alpha = 0.0124\ s^{-1}$ from NMR data
$r_1/\theta_\alpha = 0.0123\ s^{-1}$ from TPSR data

precursor, θ_b/θ_1. For each model, a relationship can be derived between k_t and θ_b/θ_1 (see Appendix). Plots of k_t vs θ_b/θ_1 for each model are shown in Fig. 11. Since the measured parameters are not known exactly, each model defines an area instead of a single line. Model I is limited to the ordinate, since all of the C_α is considered the precursor to methane. For Model III, k_t is not a function of θ_b/θ_1 since the two pools are not coupled in the model.

The steady-state experimental data can be represented as a plot of k_t versus θ_b/θ_1 in the following manner. The rate coefficient for methanation, k_t, is defined as the rate of methanation, r_1, divided by the coverage of methane precursor, θ_1:

$$k_t = \frac{r_1}{\theta_1} = \frac{r_1}{\theta_\alpha}\left[1 + \frac{\theta_b}{\theta_1}\right] \qquad (1)$$

Since only θ_α, the total coverage by C_α, can be determined experimentally and not θ_1, Eq. 1 is rearranged so that k_t is expressed in terms of r_1/θ_α and θ_b/θ_1. To plot k_t versus θ_b/θ_1 requires knowledge of r_1/θ_α. This ratio was determined from two separate experiments differing only in the reactor space velocity. In one of the experiments, θ_α was determined by integration of the broad NMR peak centered at 346 ppm, while in the other, θ_α was determined from the integral of the TPSR peak centered at 388 K, under the assumption of a symmetric peak shape. As seen in Table 2, the values of r_1/θ_α calculated in both cases are nearly equivalent.

Figure 11 shows the plot of k_t versus θ_b/θ_1 obtained from Eq. 1. For any of the models to be consistent with the experimental results, the area defined by a given model must overlap the line defined by the steady-state data. Figure 11 shows that Model II is inconsistent with the experimental data over the entire range of θ_b/θ_1. Model I and Model III are both consistent with the experimental data. From the intersection of Model III and the line representing the experimental data, a range of 2.0 to 3.5 is predicted for θ_b/θ_1.

A more rigorous test of the models is the extent to which they reproduce the transient response data shown in Fig. 4. The rate of labeled methane, r_1^* as a function of

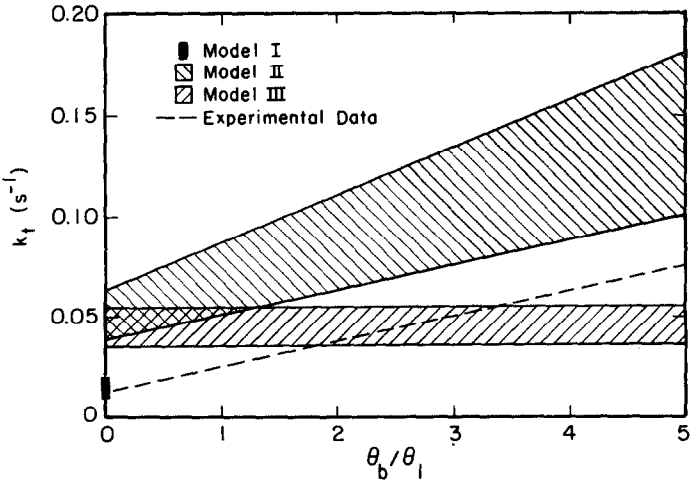

FIG. 11. Comparison of model predictions with steady-state experimental data.

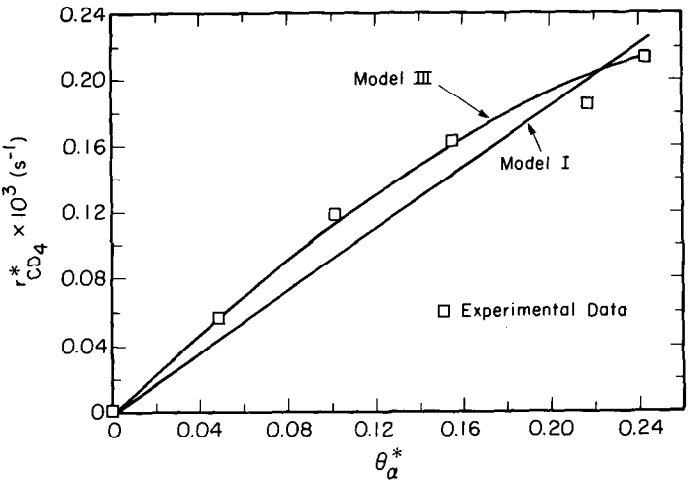

FIG. 12. Comparison of model predictions of labeled methanation rate observed as a function of θ_α measured based on data presented in Fig. 4.

θ_α* is plotted in Fig. 12. The coverage of $^{13}C_\alpha$ is determined by assuming a symmetric peak centered at 388 K. Model II is unable to predict the experimental data for any reasonable set of parameter values and is not shown in Fig. 12. Model I does not represent the data points accurately. By contrast, Model III provides an excellent fit to the experimental data. The fitted parameter values of $k_t = 0.044\ s^{-1}$ and $\theta_b/\theta_1 = 3.9$ are in good agreement with the value of $k_t = 0.044\ s^{-1}$ calculated from $t_{1/2}$ and the range of θ_b/θ_1 calculated from the steady-state data. The average lifetime on the surface of the methane precursor, τ_1, and the monomer carbon building block, τ_b, are estimated to be 7 s and 12.4 s, respectively. For $\alpha = 0.69$, the surface coverage of alkyl intermediates is about twice the coverage of θ_1 (see Appendix, Eq. A7). Using the values of $\theta_\alpha = 0.25$ and $\theta_b/\theta_1 = 3.9$, the surface coverage of alkyl intermediates is estimated to be 0.1.

The values of θ_1, τ_1, τ_b, and the coverage of alkyl intermediates estimated above can be compared with estimates of these or similar quantities reported by Biloen and coworkers (*8, 9*) and Mims *et al.* (*12, 13*) for Ru/Al_2O_3. For $T = 483$ K, $P_{H_2} = 2.55$ atm, and $P_{CO} = 0.45$ atm, Biloen *et al.* (*8*) estimated that $\theta_1 = 0.13$–0.14. This value of θ_1 is roughly twice that found in this study, $\theta_1 = 0.05$, possibly because of the higher H_2/CO ratio and total pressure used by Biloen *et al.* (*8*). In studies by Zhang and Biloen (*9*) conducted at $T = 483$ K, $P_{H_2} = 0.75$ atm, $P_{CO} = 0.25$ atm, τ_1 and τ_b were estimated to be less than 0.5 and 1.5 s, respectively. While the present results show that $\tau_b > \tau_1$, both time constants are roughly tenfold higher than those reported by Zhang and Biloen (*9*). At least a part of this difference might be due to the lower temperature (463 K) at which the present studies were conducted. The surface coverage by growing hydrocarbon chains was estimated by Mims *et al.* (*12, 13*) to be under 0.01 for the reaction conditions of $T = 455$ K, $P_{H_2} = 0.5$ atm, and $P_{CO} = 0.5$ atm. This is a factor of 10 smaller than the estimate obtained in the present study. Since the reaction conditions and the method of estimating the surface coverage of growing chains used by Mims *et al.* (*12, 13*) were significantly different from those used in this study, no clearcut explanation can be given for the differences between the two estimates.

The agreement of Model III with the ex-

perimental data still leaves the question of the nature of the building blocks for chain growth and the manner in which these species are distinguishable from the precursors for chain growth. As shown in Fig. 3, NMR spectroscopy provides evidence for only one pool of carbidic carbon. This suggests that the species composing the pools represented by θ_l and θ_b are similar. Further speculation about the identity of the species in the two pools or the nature of the sites on which each species occurs cannot be made until additional information is available.

As already noted, the present results for Ru/TiO_2 show many similarities to those presented earlier by Winslow and Bell (*2, 6*) for Ru/SiO_2. Both catalysts show the build up of C_α and C_β with time under reaction conditions and the NMR spectra of the species show no dependence on the nature of the support. The principal differences between Ru/TiO_2 and Ru/SiO_2 are in activity and level of carbon accumulation. For a fixed set of conditions (463 K, P_{D_2} = 150 Torr, and P_{CO} = 50 Torr), the turnover frequency for Ru/TiO_2 is 4.0×10^{-3} s^{-1}, whereas that for Ru/SiO_2 is 8.1×10^{-4} s^{-1} (*2*). A part of the fivefold higher activity of Ru/TiO_2 can be ascribed to its lower dispersion: D_{Ru} = 0.12 for Ru/TiO_2 and D_{Ru} = 0.27 for Ru/SiO_2. If the activity of Ru/SiO_2 is adjusted to correspond to D_{Ru} = 0.12 using the data of Kellner and Bell (*30*), the turnover frequency would be 1.6×10^{-3} s^{-1}. In addition to exhibiting a higher activity, Ru/TiO_2 also exhibits a higher accumulation of C_α. For the reaction conditions indicated above, θ_α = 0.25 for Ru/TiO_2 and θ_α = 0.01 for Ru/SiO_2, at steady state.

The higher activity and C_α coverage of Ru/TiO_2 relative to Ru/SiO_2 can be ascribed to the effects of support composition (*23*). Previous studies with Rh (*31, 32*), have shown that even under low-temperature-reduction conditions, TiO_2-supported Rh is significantly more active than Rh dispersed on other supports. While not proven definitively, the higher activity of Rh/TiO_2 has been attributed to the presence of small islands of TiO_x on the surface of the dispersed metal particles. Studies in this laboratory with TiO_2-promoted Rh foil and Pd/SiO_2 (*33, 34*) have shown that even small amounts of TiO_x enhance the CO hydrogenation activity of the metal and promote the dissociation of adsorbed CO to carbon and oxygen. It is, therefore, quite plausible that similar effects are responsible for the differences between Ru/TiO_2 and Ru/SiO_2.

CONCLUSIONS

The results of this investigation show that under reaction conditions, the surface of titania-supported Ru is covered by carbon monoxide, carbidic carbon, and alkyl chains. The CO, in equilibrium with the gas phase, dominates the surface. The carbidic carbon, which covers about 25% of the surface, is divided into two separate species, a methane precursor (20%) and a monomer building block for chain growth (80%). Both the methane precursor and the monomer building block are formed directly from adsorbed CO. The majority of the alkyl chains present on the catalyst are not reaction intermediates and accumulate on the support as the reaction proceeds. An estimated 10% of the surface is covered by alkyl chains which are the precursors to C_{2+} hydrocarbon products.

APPENDIX

The assumptions and derivations of the equations used to generate Figs. 11 and 12 are presented below. The following assumptions are made. Carbon monoxide is assumed to be in equilibrium with the gas phase. The turnover number for formation of hydrocarbon chains of length n, r_n, can be expressed as

$$r_n = k_t \theta_n, \qquad \text{(A1)}$$

where θ_n is the fractional coverage of the Ru surface by alkyl groups of chain length n and k_t is the rate coefficient for chain termination. It is further assumed that the rate of

chain propagation of alkyl groups of length n can be written as

$$r_p = k_p \theta_b \theta_n, \tag{A2}$$

where k_p is the rate coefficient for chain propagation and θ_b is the fractional coverage of the Ru surface by the monomer carbon building block for chain growth. The rate coefficients for chain propagation, k_p, and chain termination, k_t, are assumed to be independent of chain length. The probability of chain growth, α, is then expressed as

$$\alpha = (k_p \theta_b)/(k_t + k_p \theta_b). \tag{A3}$$

Each carbon pool, θ_n, is assumed to be internally homogeneous, i.e., characterized only by the lifetime of that species on the catalyst surface, τ_n.

The following relationships can easily be derived from the assumptions given above:

$$\theta_n = \alpha^{n-1} \theta_1 \tag{A4}$$

$$\sum_{n=1}^{\infty} \alpha^{n-1} = \frac{1}{1-\alpha} \tag{A5}$$

$$\sum_{n=1}^{\infty} n\alpha^{n-1} = \frac{1}{[1-\alpha]^2} \tag{A6}$$

$$\theta_1 = \frac{1-\alpha}{\alpha} \sum_{n=2}^{\infty} \theta_n. \tag{A7}$$

For each model, the labeled methanation rate, r_1^*, is calculated as a function of time after a switch made from unlabeled ^{12}CO and D_2 to labeled ^{13}CO and D_2. The isotopic switch is modeled as a step function change in the isotopic composition of the adsorbed CO. For Models I and III, the reaction pathway for methane formation passes through only one monomer carbon pool. The response of a single carbon pool is equivalent to the response of a CSTR, i.e., a simple exponential increase in the amount of labeled carbon, θ_1^*, with a time constant, τ_1. The labeled rate of methanation, r_1^* can be expressed as

$$r_1^* = r_{\text{final}}^* [1 - e^{-t/\tau_1}], \tag{A8}$$

where $r_{\text{final}}^* = r_1^*$ $(t \to \infty)$. For Model II, the reaction pathway for methane passes through two pools of monomer carbon, θ_b and θ_1, which are connected in series. The response is equivalent to that of two CSTRs connected in series, with time constants τ_b and τ_1. For Model II, r_1^* can be written as

$$r_1^* = r_{\text{final}}^* \left[1 - \frac{\tau_b}{\tau_b - \tau_1} e^{-t/\tau_b} + \frac{\tau_1}{\tau_b - \tau_1} e^{-t/\tau_1}\right]. \tag{A9}$$

The rate at which CO reacts, r_{CO}, is equal to the rate at which hydrocarbons are produced:

$$r_{CO} = \sum_{n=1}^{\infty} n r_n. \tag{A10}$$

r_{CO} can be expressed in terms of k_t and α by combining Eqs. (A1), (A4), (A6), and (A10):

$$r_{CO} = k_t \theta_1/(1-\alpha)^2. \tag{A11}$$

For each model, the time constants τ_1 and τ_b are expressed in terms of the model parameters, α, k_t, and θ_b/θ_1. For Model I, all the CO which reacts must pass through the monomer carbon pool. Thus the flux of carbon atoms through the monomer carbon pool, θ_1/τ_1, is equal to the rate at which CO reacts given in Eq. (A11). Hence

$$\theta_1/\tau_1 = k_t \theta_1/(1-\alpha)^2. \tag{A12}$$

Solving for τ_1 yields

$$\tau_1 = (1-\alpha)^2/k_t. \tag{A13}$$

For Models II and III, the flux of carbon atoms through θ_1 is equal to the rate of conversion of θ_1 to methane plus the rate at which θ_1 initiates the growing chains. The flux through the methane precursor pool, θ_1/τ_1, can be written as

$$\theta_1/\tau_1 = k_t \theta_1 + k_p \theta_b \theta_1. \tag{A14}$$

Solving for τ_1 using Eqs. (A3) and (A14) results in Eq. (A15).

$$\tau_1 + (1-\alpha)/k_t. \tag{A15}$$

For Model II, all the CO which reacts must pass through pool θ_b. Thus, the flux of carbon atoms, θ_b/τ_b, is equal to r_{CO}. Solving for τ_b results in

$$\tau_b = (\theta_b/\theta_1)(1 - \alpha)^2/k_t. \quad \text{(A16)}$$

For Model III, all the CO which reacts must pass through either pool θ_1 or pool θ_b. This implies that

$$\theta_1/\tau_1 + \theta_b/\tau_b = r_{CO}. \quad \text{(A17)}$$

Using Eqs. (A11), (A15), and (A17), τ_b can be expressed as

$$\tau_b = \frac{\theta_b}{\theta_1}\frac{(1-\alpha)^2}{\alpha k_t}. \quad \text{(A18)}$$

The rate coefficient for termination, k_1, can be expressed as a function of θ_b/θ_1 using Eqs. (A13), (A15), and (A16) with the rate expressions for r_1^* (Eqs. (A8) and (A9)) and the definition of the half-life, $r_1^*(t_{1/2}) = 0.5$. The results of this calculation are presented in Fig. 11.

For each model the rate of labeled methanation, r_1^*, as a function of θ_α^* is determined. For Model I, all of the C_α serves as a methane precursor. This implies that

$$r_1^* = k_t\theta_1^* = k_t\theta_\alpha^*. \quad \text{(A19)}$$

Since only the total coverage of labeled monomer carbon, θ_α^*, is known as a function of time, the amount of labeled methane precursor, θ_1^*, must be calculated for Models II and III. The magnitude of θ_1^* is given by

$$\theta_1^* = \theta_\alpha^*/[1 + \theta_b^*/\theta_1^*]. \quad \text{(A20)}$$

The isotopic fraction of θ_b varies as a simple exponential with time constant τ_b:

$$\theta_b^* = \theta_b[1 - e^{-t/\tau_b}]. \quad \text{(A21)}$$

The isotopic composition of the methane precursor as a function of time has already been solved in Eq. (A8) for Model III and Eq. (A9) for Model II. For Model II, by combining Eqs. A1, A9, A20, and A21, r_1^* can be written as

$$r_1^* = k_t\theta_\alpha^* \Bigg/ \left[1 + \frac{\theta_b[1 - e^{-t/\tau_b}]}{\theta_1\left[1 - \frac{\tau_b}{\tau_b - \tau_1}e^{-t/\tau_b} + \frac{\tau_1}{\tau_b - \tau_1}e^{-t/\tau_1}\right]}\right]. \quad \text{(A22)}$$

For Model III, using Eqs. (A1), (A8), (A20), and (A22), r_1^* can be expressed as

$$r_1^* + k_t\theta_\alpha^* \Big/ \left[1 + \frac{\theta_b[1 - e^{-t/\tau_b}]}{\theta_1[1 - e^{-t/\tau_1}]}\right]. \quad \text{(A23)}$$

Figure 12 presents the labeled methanation rate, r_1^*, as a function of θ_α^* measured at different times after a switch from $^{12}CO/D_2$ to $^{13}CO/D_2$ (see Fig. 4). The three models are fit to the experimental points using Eqs. (A19), (A22), and (A23) by varying the values of k_t and θ_b/θ_1. The expressions for τ_b and τ_1 used to fit the data are given by Eqs. (A13), (A15), (A16), and (A18).

ACKNOWLEDGMENTS

This work was supported by the Division of Chemical Sciences, Office of Basic Energy Sciences, U.S. Department of Energy, under Contract DE-AC03-76SF00098 and by Exxon Research and Engineering Company. The authors also wish to thank Dr. T. M. Duncan for acquiring the NMR spectra shown in Figs. 3 and 6.

REFERENCES

1. Cant, N. W., and Bell, A. T., *J. Catal.* **73,** 257 (1982).
2. Winslow, P., and Bell, A. T., *J. Catal.* **86,** 158 (1984).
3. Winslow, P., and Bell, A. T., *J. Catal.* **91,** 142 (1985).
4. Duncan, T. M., Winslow, P., and Bell, A. T., *J. Catal.* **93,** 1 (1985).
5. Duncan, T. M., Reimer, J. A., Winslow, P., and Bell, A. T., *J. Catal.* **93,** 305 (1985)
6. Winslow, P., and Bell, A. T., *J. Catal.* **94,** 385 (1985).
7. Biloen, P., *J. Mol. Catal.* **21,** 17 (1983).
8. Biloen, P., Helle, J. N., van den Berg, F. G. A., and Sachtler, W. M. H., *J. Catal.* **81,** 450 (1983).
9. Zhang, X., and Biloen, P., *J. Catal.* **98,** 468 (1986).
10. Mims, C. A., and McCandlish, L. E., *J. Amer. Chem. Soc.* **107,** 696 (1985).
11. Mims, C. A., and McCandlish, L. E., *J. Phys. Chem.* **91,** 929 (1987).

12. Mims, C. A., McCandlish, L. E., and Melchior, M. T., *Catal. Lett.* **1,** 121 (1988).
13. Mims, C. A., McCandlish, L. E., and Melchior, M. T., *in* "Proceedings, 9th International Congress on Catalysis, Calgary, 1988" (M. J. Phillips and M. Ternen, Eds.), Vol. 4, p. 1992. Chem. Institute of Canada, Ottawa, 1988.
14. Stockwell, D. M., Bianchi, D., and Bennett, C. O., *J. Catal.* **113,** 13 (1988).
15. Dalla Betta, R. A., and Shelef, M., *J. Catal.* **48,** 111 (1977).
16. King, D. L., *J. Catal.* **61,** 77 (1980).
17. Ekerdt, J. G., and Bell, A. T., *J. Catal.* **58,** 170 (1979).
18. Kellner, C. S., and Bell, A. T., *J. Catal.* **71,** 296 (1981).
19. Yamasaki, H., Kobori, Y., Naito, S., Onishi, T., and Tamaru, K., *J. Chem. Soc. Faraday Trans. 1* **77,** 2913 (1981).
20. Kobori, Y., Yamasaki, H., Naito, S., Onishi, T., and Tamaru, K., *J. Chem. Soc. Faraday Trans. 1* **78,** 1473 (1982).
21. Fukushima, T., Fujimoto, K., and Tominaga, H., *Appl. Catal.* **14,** 95 (1985).
22. Zhou, X., and Gulari, E., *in* "Proceedings, 3rd China–Japan–US Symposium on Catalysis, Xiamen, People's Republic of China, 1987," paper B-30.
23. Nice, M., and Garten, R. L., *J. Catal.* **63,** 255 (1980).
24. Hicks, R. G., Kellner, C. S., Savatsky, B. J., Hecker, W. C., and Bell, A. T., *J. Catal.* **71,** 216 (1981).
25. Underwood, R. P., and Bell, A. T., *Appl. Catal.* **21,** 157 (1986).
26. Abrevaya, H., Targos, W. M., Robota, H. J., and Cohn, M. J., *in* "Proceedings, 10th Meeting North American Catalyst Society San Diego, 1987" (J. W. Ward, Ed.), paper A40.
27. Wakui, T., and Handa, T., *J. Chem. Soc. Chem. Comm.*, 994 (1984).
28. Zhou, X., and Gulari, E., *J. Catal.* **105,** 499 (1987).
29. Akhter, S., and White, J. M., *Surf. Sci.* **180,** 19 (1987).
30. Kellner, C. S., and Bell, A. T., *J. Catal.* **75,** 251 (1982).
31. Katzer, J. R., Sleight, A. W., Gajardo, P., Michels, J. B., Gleason, E. F., and McMillan, S., *Faraday Discuss. Chem. Soc.* **72,** 121 (1981).
32. Haller, G. L., Heinrich, V. E., McMilland, M., Resaco, D. E., Sadeghi, H. R., and Sakellson, S., *in* "Proceedings, 8th International Congress on Catalysis, Berlin, 1984," Vol. 5, p. 135. Dechema, Frankfurt-am-Main, 1984.
33. Levin, M. E., Salmeron, M., Somorjai, G. A., and Bell, A. T., *J. Catal.* **106,** 401 (1987).
34. Rieck, J. S., and Bell, A. T., *J. Catal.* **99,** 262 (1986).